

Metal-Water mixtures for Propulsion and Energy-Conversion Applications: Recent Progress and Future Directions

D. Sundaram

Indian Institute of Technology Gandhinagar, Palaj, Gandhinagar, Gujarat, 382355, India

Article info

Received:
15 July 2017

Received in revised form:
26 September 2017

Accepted:
18 November 2017

Abstract

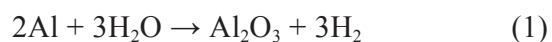
The metal-water system is attractive for propulsion and energy-conversion applications. Of all metals, aluminum is attractive due to its high energy density, relative safety, and low cost. Experimental studies provide new insight on the combustion and propulsive behaviors. The burning rate is found to be a strong function of both pressure and particle size. Furthermore, there is a wide scatter in the measured pressure exponents due to differences in particle size, pressure, pH, and equivalence ratio. A major problem with Al/H₂O mixtures is incomplete combustion and poor impulses, thereby rendering Al/H₂O mixtures unsuitable for practical applications. Efforts to improve the performance of Al/H₂O mixtures have only met with moderate success. Although experiments have revealed these new trends, not much is offered in terms of the underlying physics and mechanisms. To explore the combustion mechanisms, theoretical models based on energy balance analysis have been developed. These models involve numerous assumptions and many complexities were either ignored or treated simplistically. The model also relies on empirical inputs, which makes it more a useful guide than a predictive tool. Future works must endeavor to conduct a more rigorous analysis of metal-water combustion. Empirical inputs should be avoided and complexities must be properly treated to capture the essential physics of the problem. The model should help us properly understand the experimental trends, offer realistic predictions for unexplored conditions, and suggest guidelines and solutions in order to realize the full potential of metal-water mixtures.

1. Introduction

Metal particles are of concern to propulsion and energy-conversion applications [1]. Of all metals, aluminum (Al) in the form of micron-sized particulates is commonly used due to its high energy density, low cost, and relative safety [2]. Ignition of micron-sized and larger Al particles occurs at temperatures as high as 2350 K upon melting of the oxide layer [3]. The high ignition temperatures and particle agglomeration lowers the energy-release rates in many practical applications [1]. Nanoparticles possess unique and favorable properties due to the greater percentage of atoms of the surface and excess energy of the surface atoms. For example, the ignition temperature of aluminum particles decreases with decreasing particle size, from about 2350 K at 100 μm to 933 K at 100 nm [2]. Sub-

stantial enhancements in burning rates have thus been achieved when metal nanoparticles are used instead of micron-sized counterparts in energetic materials [4].

Recently, there has been an enormous interest in metal-water for a number of reasons. Firstly, the mixture is quite simple in composition and is relatively safe to handle [5]. Aluminum, a candidate metal, is the most abundant metal in Earth's crust and water covers nearly 70% of the Earth's surface. Secondly, the metal-water reaction is quite exothermic and the mixture is thus associated with large energy content. The aluminum-water reaction is given by



The enthalpy of reaction is about 813 kJ. For comparison, the enthalpy of H₂/O₂ reaction is about

*Corresponding author. E-mail: dilip.sundaram@iitgn.ac.in

242 kJ. On a gravimetric basis, enthalpies of combustion of Al/H₂O and H₂/O₂ systems are about 7 and 13 kJ/g of mixture, respectively. However, on a volumetric basis, the enthalpies of combustion of Al/H₂O and H₂/O₂ systems are about 11 and 5.6 kJ/cm³, respectively. It is apparent that metal-water mixtures are quite useful for volume-limited applications. Another advantage is that the combustion products are environmentally benign, unlike conventional composite solid rocket propellants (such as AP/HTPB) [1].

The Al/H₂O reaction is of relevance for a number of applications. In a typical aluminized composite solid propellant, aluminum particles react with the combustion products of the base propellant, which mainly consists of carbon dioxide and water vapor [6]. As a result, understanding of Al/H₂O reaction is expected to help understand the overall propellant combustion [7]. Since one of the major products of Al/H₂O reaction is hydrogen, the mixture is also viewed as a chemical source of hydrogen and is thus considered for hydrogen generation applications [8]. It is also of interest to underwater propulsion, since the oxidizer (water) need not be carried on-board [9]. Furthermore, the propellant can be manufactured in other water-bearing planets instead of being transported at a huge cost [7]. These factors have generated tremendous interest in the Al/H₂O system.

In this paper, the thermochemical behavior of Al/H₂O system is first characterized. Recent progress in experimental and theoretical studies is then reviewed. Deficiencies in the knowledge base are identified and directions for future work are suggested.

2. Thermochemical characterization

The thermodynamic performance of Al/H₂O mixtures is characterized by NASA chemical equilibrium with applications (CEA) program [10]. One of the most important thermochemical parameters is the adiabatic flame temperature. Figure 1 shows the effect of oxidizer-fuel weight (O/F) ratio on the adiabatic flame temperature of Al/H₂O mixtures. For pure Al/H₂O mixtures, the adiabatic flame temperature increases with increasing O/F ratio and attains a maximum value of about 2850 K at O/F ratio of unity. This is not surprising since the stoichiometric Al/H₂O mixture consists of equal mass of aluminum and water. Calculations are also performed for mixtures containing nanoparticles to quantify the effect of oxide layer on the flame

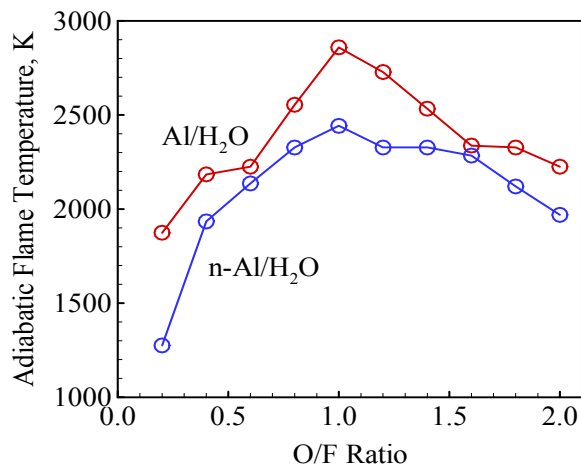


Fig. 1. Effect of oxidizer-fuel weight (O/F) ratio on the adiabatic flame temperature of Al/H₂O mixtures; oxide content in nanoparticles is 50% by mass.

temperature. The particle size is chosen to be 40 nm and the resulting oxide layer content is about 50% by mass of the particle. As the oxide layer is an inert material, the adiabatic flame temperature drops from about 2850 to 2450 K for O/F ratio of unity. Figure 2 shows the effect of pressure on the adiabatic flame temperature of stoichiometric mixtures. The variation of boiling point of aluminum with pressure is obtained using the Clausius-Clapeyron equation. For pressures representative of those in practical propulsion applications, the adiabatic flame temperature is lower than the boiling point of aluminum. As a result, vaporization of aluminum is unlikely to occur and combustion must take place via heterogeneous surface reactions. This is more so for n-Al/H₂O mixtures due to their lower adiabatic flame temperatures.

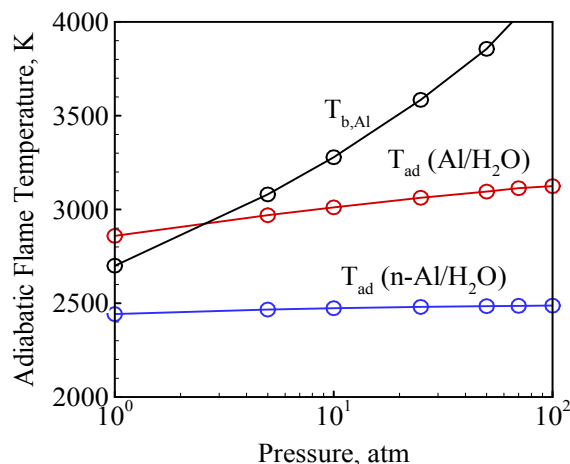


Fig. 2. Effect of pressure on the adiabatic flame temperature of stoichiometric Al/H₂O mixtures; oxide content in nanoparticles is 50% by mass.

An important metric of efficiency of rocket propellants is the specific impulse. It represents the thrust force per unit mass burning rate of the propellant. The specific impulse of a propellant is directly related to the nozzle exit velocity [11]:

$$V_c = \sqrt{\frac{2k}{k-1} \frac{R_u}{MW} T_c \left[1 - \left(\frac{p_e}{p_c} \right)^{\frac{k-1}{k}} \right]}, \quad (2)$$

where k is the adiabatic constant, R_u the universal gas constant, MW the molecular weight of product gases, T_c the combustion temperature, and p the pressure. The subscripts e and c refers to nozzle exit and combustion chamber, respectively. The specific impulse can be increased by increasing the combustion temperature and decreasing the molecular weight of exhaust gases. Figures 3 and 4 shows the sea-level specific impulse of Al/H₂O propellants for different O/F ratios (or equivalence ratios). Calculations were performed using the NASA CEA code [10]. The chamber pressure is 50 atm and the gas is expanded to atmospheric pressure. To understand the specific impulse trends, it is important to understand the effect of O/F ratio on adiabatic flame temperature and product molecular weight. For pure Al/H₂O propellant, the adiabatic flame temperature takes a maximum value of ~3100 K for O/F ratio of unity due to the right balance between aluminum and water. Beyond O/F = 1, molecular weight decreases, since there is more unreacted water in the products and water has lower molecular weight than the mean molecular weight of alumina and hydrogen.

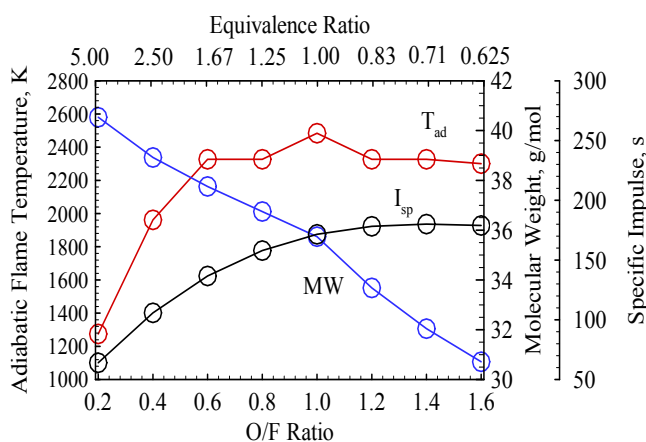


Fig. 3. Sea-level specific impulse, adiabatic flame temperature, and product molecular weight of Al/H₂O propellant as a function of O/F ratio; theoretical calculations for a chamber pressure of 50 atm and product expanded to atmospheric pressure.

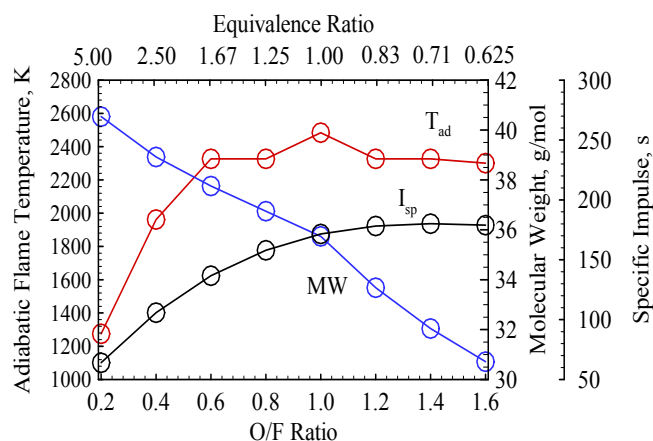


Fig. 4. Sea-level specific impulse, adiabatic flame temperature, and product molecular weight of n-Al-H₂O propellant as a function of O/F ratio; theoretical calculations for a chamber pressure of 50 atm, particle oxide content of 50 wt.%, product expanded to atmospheric pressure.

On the other hand, no such reduction is observed for O/F ratios lower than unity, as the molecular weight of unreacted aluminum is equal to the mean molecular weight of alumina and hydrogen. For these reasons, a maximum specific impulse of about 225 sec is predicted for stoichiometric/slightly fuel-lean mixtures.

The situation becomes different for Al/H₂O mixture containing nanoparticles. The oxide layer content in the particle is taken as 50%. Note that the maximum flame temperature is around 2500 K, lower than that of pure Al/H₂O propellant due to the high oxide content in the particles. The product molecular weight is also higher, since alumina has the highest molecular weight of 102 g/mol among all major species of concern. Furthermore, for fuel-rich mixtures, the molecular increases with decreasing O/F ratio, since the unburned aluminum particles are associated with high oxide content. The peak specific impulse is attained for slightly fuel-lean conditions, as the molecular weight exerts a slightly stronger effect than the flame temperature near stoichiometric condition. Note however that the peak specific impulse is 178 sec, lower than that of pure Al/H₂O system (225 sec).

Table 1 compares the sea-level specific impulse of Al/H₂O propellants with those of conventional solid and liquid propellants. Note that the actual impulse is typically lower due to inefficiencies associated with combustion and expansion processes. Although the specific impulse is greatest for LOX/LH₂ propellants, it is comparable for pure Al/H₂O propellants and conventional aluminized

solid propellants. Note that the oxide content in the particles is detrimental to the specific impulse. The density impulses of Al/H₂O propellants are however greater than those of the two liquid propellants considered here due to greater propellant densities. This is likely to result in significant savings in the tank mass and increase in the payload capacity.

Table 1

Comparison of sea-level specific impulses of different propellants; theoretical calculations for a chamber pressure of 50 atm and product expanded to atmospheric pressure

Propellant	Density (g/cm ³)	I _{sp} , sec	I _{sp} , g-s/cm ³
LOX/LH ₂	0.361	370	133
(O/F = 6.0)			
LOX/RP-1	1.02	290	296
(O/F = 2.38)			
AP/Al/HTPB	1.82	256	466
(68/20/12)			
Al/H ₂ O	1.459	225	329
n-Al/H ₂ O	1.758	180	316

3. Experimental studies

One of the first experimental studies on nanoaluminum-water combustion was conducted by Ivanov et al. in 1994 [12]. Ultra-disperse Al particles produced by electric explosion of wires were mixed with distilled water under stoichiometric conditions. Although the particle size was reported to be 1 μm, the specific surface area was 18 m²/g. The mixture was gelled by adding polyacrylamide (~3%). The study was conducted in a constant-pressure vessel using 10 mm diameter quartz beakers in an argon environment. Burning rates were measured over a pressure range of 0.1–7 MPa. The measured burning rates were described by the following correlation [12]:

$$r_b [\text{cm/s}] = 0.183(p[\text{MPa}]/p_0)^{0.4}, \quad (3)$$

where p_0 is the baseline pressure of 0.1 MPa. However, mechanisms of combustion were not explored and no attempt was made to explain the observed burning-rate trend.

In a subsequent study [13], detailed characterization of Al/H₂O combustion was attempted using the same experimental setup. The temperature profile was obtained using thermocouples. The particle size was reported to be 120 nm, which is consistent with the high specific surface area of the

Al powder (18 m²/g). The active aluminum content was 96.5%. The combustion efficiencies were about 50–60% over a pressure range of 0.1–7 MPa. Incomplete combustion was attributed to boiling out phenomenon of water. After vaporization, water vapor accelerates and exits the tube and is thus not easily available to oxidize Al particles. To validate this claim, the authors considered a fuel-lean mixture (40% Al and 60% water) with the hope that the excess water would result in a more complete combustion of Al particles. For fuel-lean mixtures, the combustion efficiency reached 99% at a pressure of 5 MPa and the combustion temperatures were as high as 2400 K. For comparison, the maximum combustion temperature was about 2100 K for the stoichiometric mixture. Similarly, the burning rate was about 1.7 cm/s at 7 MPa, significantly greater than the counterpart of the stoichiometric mixture. These observations support the “boiling-out” theory.

While studies of Ivanov et al. used a gelling agent to achieve self-sustained combustion, Risha et al. [7] was able to achieve self-sustained combustion without any gelling agent. Steady burning rates were measured using a windowed pressure vessel, as shown in Fig. 5 [5]. The 61 cm long stainless steel chamber has an inner diameter of 22 cm and a total free volume of 23 l to minimize the pressure variation caused by the generation of gaseous combustion products. Aluminum nanoparticles were mixed with distilled water in a sealed plastic bag. The mixture was then packed into a quartz glass tube (1 cm OD, 0.8 cm ID, 7.5 cm long) and ignited. The temporal evolution of the flame front, tracked and recorded using video equipment, was used to obtain the burning rate.

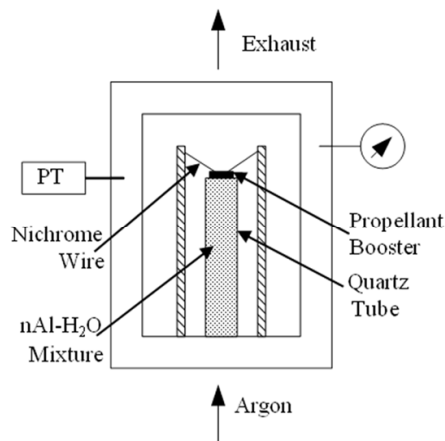


Fig. 5. Schematic of the constant-pressure strand burner with optical access (reprinted from [5] with permission of Elsevier).

Figure 6 shows the effect of pressure on the burning rate of 80 nm Al/H₂O mixtures [14]. Pressure exponents are in the range of 0.27–0.40, depending on the thermodynamic state of water. The burning rate was found to be inversely proportionally to particle size over a size range of 50–130 nm [7]. Both diffusion and chemical kinetics were speculated to affect the burning rate [7], but key mechanisms and processes were not understood.

A similar study was also conducted by Shafirovich et al. [8] and they obtained a value of about 2 mm/s for a particle size of 80 nm and pressure of 1 atm. The combustion efficiency was reported to be 50%, suggesting that incomplete combustion resulted in a low burning rate. In a follow-up work [15], Risha et al. measured chemical conversion efficiencies of Al/H₂O mixtures using a constant volume closed chamber. Based on the hydrogen concentration after the test, conversion efficiencies were determined. Measured conversion efficiencies were in the range of 27–99%. Increasing the pressure, mixture confinement, and decreasing the particle size resulted in higher conversion efficiencies.

In subsequent studies, Al/H₂O combustion was further studied in an attempt to capture the details of the combustion process and effect of process parameters. Firstly, the effect of pH was explored [16]. The value of the pH, moderated using HCl, had a profound effect on the mixture consistency. pH close to 7.0 resulted in aggregation or clustering of particles due to strong inter-particle attractive forces. On the other hand, lower or higher pH values resulted in fluid-like consistency (with dispersed particles) due to repulsion forces caused by the formation of ionic charge clouds at the solid-liquid interface. The pressure exponent in the burning rate took values of 0.68, 0.58, and 0.34

for pH values of about 9, 3, and 5, respectively. A connection between propellant consistency and pressure exponent was thus established.

The effect of equivalence ratio was also studied [17]. The combustion efficiency increased with decreasing equivalence ratio, from about 70% at $\phi = 1$ to 95% at $\phi = 0.67$. This is in agreement with the findings of Ivanov et al. [13]. However, the burning rate and pressure exponent were not significantly affected by the equivalence ratio. Unburned aluminum agglomerates were observed for stoichiometric mixtures. It was proposed that the combustion of Al/H₂O mixtures is controlled by mass diffusion due to the presence of large agglomerates.

The Al/H₂O mixture has been refrigerated (by freezing the water in the mixture) and the propulsive performance of the resulting solid propellant (ALICE) has been characterized [14]. Laboratory-scale static fire motor experiments were conducted for motors with three different combustion chamber diameters of 1.91, 3.81, and 7.62 cm. A post combustion chamber with a length of 7.62 cm was used. Both center-perforated and end-burning motors were employed. Three different grain lengths of 3.81, 7.62, and 15.2 cm were considered for end-burning motors. For center-perforated motors, the grain length was chosen as 7.62 cm. A graphite nozzle with a contraction ratio of 10 and divergence half-angle of 15 degrees was used. The instantaneous thrust was measured using an OMEGA load cell. Table 2 shows the propulsive performance of the ALICE propellant [14]. The specific impulse varies in the range of 56–133s, much lower than the theoretical estimates. The disparity was attributed to low combustion efficiencies caused by low combustion temperatures, insufficient residence time, and particle agglomeration.

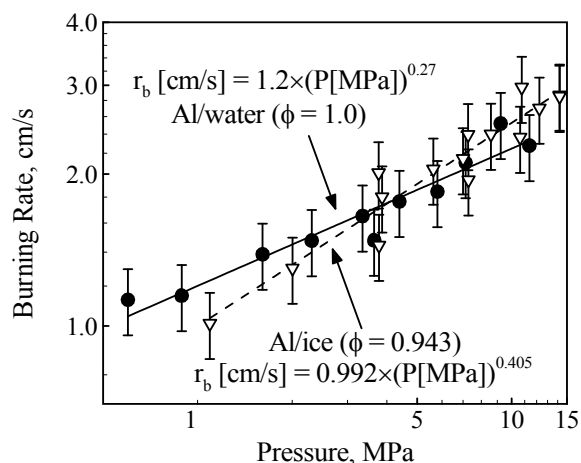


Fig. 6. Effect of pressure on the burning rate of 80 nm Al/H₂O mixture (reprinted from [14] with permission of American Institute of Aeronautics and Astronautics).

Table 2

Performance parameters for ALICE propellants at an equivalence ratio of 0.71 (reprinted from [14] with permission of American Institute of Aeronautics and Astronautics)

Parameter	Motor Size [cm]		
	1.91	3.81	7.62
Peak Thrust (N)	166	318	908
\bar{C}^* (m/s)	528	784	848
η_{C^*} (%)	43	64	96
\bar{I}_{sp} (s)	56	83	133
η_{Isp} (%)	27	40	64
Isp @ Peak Pressure (s)	97	124	203
\bar{I}_{sp} with Al ₂ O ₃ retained (s)	63	117	233

Considering the deficiencies of Al/H₂O mixtures, efforts have been made to improve the performance of aluminum-water mixtures. One of the major issues with nanoparticles is the high oxide content, which results in a low energy content. The energy content can be enhanced by using micron-sized particles, since the active aluminum content is nearly 100% [18, 19]. The burning rate, however, decreases by a factor of four when the loading density of micron-sized particles increases from 0 to 80% due to poor reactivity of micron-sized particles [19]. Another approach to enhance the energy content is using hydrogen peroxide instead of water [20, 21]. It is well known that the heat of Al–H₂O₂ reaction is 1388 kJ/mol, which is nearly twice that of Al–H₂O counterpart (813 kJ/mol). As a result, a substantial enhancement of the burning rate is observed [20, 21]. Aluminum hydride (alane) has also been considered to enhance the hydrogen content of the mixture [18].

4. Theoretical studies

Theoretical studies on Al/H₂O combustion have been conducted to explore the underlying physics and explain the experimental observations. A 1-D flame propagation model was developed to predict the burning rates and flame structure by solving the conservation equations in each zone and matching temperature and heat flux at the interfacial boundaries [5]. The model assumed steady-state propagation, constancy of pressure, and ignored many complexities such as motion and agglomeration of particles. Figure 7 shows the physical model of concern and multi-zone flame structure [5]. The coordinate system was attached to the propagating flame. The entire region of concern was divided into three zones: (1) liquid water preheat zone; (2) water vapor preheat zone; and (3) reaction zone.

Water vaporizes at the boiling front, $x = \delta_v$, where the temperature is equal to the boiling point, T_v . The mixture begins to react once the ignition temperature, T_{ign} , is attained. Chemical reactions were neglected in the preheat zones. The governing equations and boundary conditions for each zone are presented below.

4.1. Liquid water preheat zone

The energy equation in this zone takes the form [5]

$$\left(\rho_{Al}C_{p,Al}\Phi_{Al} + \rho_{ox}C_{p,ox}\Phi_{ox} + \rho_{lw}C_{p,lw}\Phi_{lw}\right)r_b \frac{dT}{dx} = \lambda_{m,w} \frac{d^2T}{dx^2}, \quad (4)$$

subject to the boundary conditions [5]:

$$T_{x \rightarrow -\infty} = T_u; T_{x = -\delta_v} = T_v; \quad (5)$$

where ρ is the density, C_p the specific heat, r_b the burning rate, T the temperature, x the space coordinate, and δ_v the thickness of the water vapor preheat zone. The subscripts *W*, *u*, *v*, *ox*, and *lw* refer to the liquid water zone, unburned state, vaporization, oxide, and liquid water, respectively. Analytical solution of Eq. (4), subject to the boundary conditions, gives the temperature distribution in this zone, which is a function of the burning rate (the primary unknown).

4.2. Water vapor preheat zone

At the boiling front, $x = -\delta_v$, water boils and the resulting vapor flows through the interstitial space between particles. It was assumed that the particles are not entrained by the gas and the momentum conservation was thus not considered [5]. The conservation of mass of water was enforced to de-

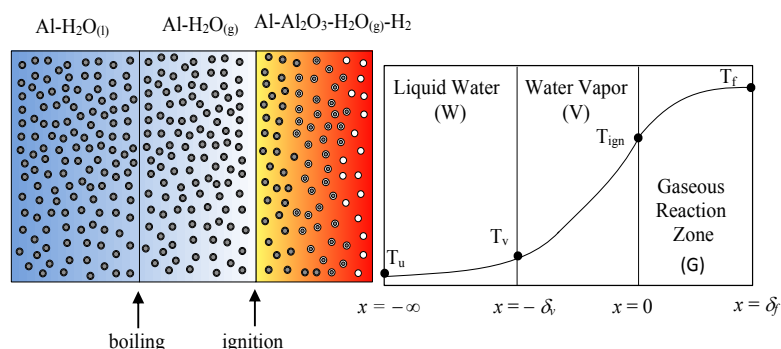


Fig. 7. Physical model and multi-zone flame structure (● Al, ○ Al₂O₃) (reprinted from [5] with permission of Elsevier).

termine the velocity of water vapor at the boiling front [5]

$$\rho_{lv}r_b = \rho_{wv}v_{wv} \quad (6)$$

Here, v is the gas velocity. The subscript wv denotes water vapor. The energy equation is given by [5]

$$\left(\rho_{Al}C_{p,Al}\Phi_{Al} + \rho_{ox}C_{p,ox}\Phi_{ox} + \rho_{lv}C_{p,wv}\Phi_{lv}\right)r_b \frac{dT}{dx} = \lambda_{m,v} \frac{d^2T}{dx^2}, \quad (7)$$

subject to the interfacial conditions [5]:

$$\begin{cases} x = -\delta_v : \lambda_m \frac{dT}{dx} \Big|_V = \lambda_m \frac{dT}{dx} \Big|_W + h_{fg} \Phi_{lv} \rho_{lv} r_b, \\ x = 0 : T = T_{ign}, \end{cases} \quad (8)$$

where h_{fg} is the enthalpy of water vaporization and T_{ign} the ignition temperature of aluminum nanoparticles. The subscript V refers to the water vapor preheat zone. The thickness of this zone was obtained by performing the heat flux balance at $x = -\delta_v$. Analytical solution of Eq. (7), subject to the boundary conditions, gives the temperature distribution. Note that the both water vapor zone thickness and temperature distribution in the water vapor preheat zone are functions of the burning rate (the primary unknown).

4.3. Reaction zone

The energy equation can be expressed as [5]

$$\left(\sum_i \rho_i C_{p,i} \Phi_i\right)r_b \frac{dT}{dx} = \lambda_{m,G} \frac{d^2T}{dx^2} + \frac{\rho_m Q_r}{\tau_b}, \quad (9)$$

where Q_r is the chemical energy release per unit mass of the mixture and τ_b the particle burning time. The subscripts G , m and i refer to the reaction zone, mixture, and species i , respectively. The heat of reaction was adjusted to account for heat losses and combustion inefficiency so as to obtain the measured combustion temperature of ~ 1800 K [5]. The ignition temperature of aluminum nanoparticles was taken to be 1360 K [5]. For the burning time, a reference burning time was employed; this was the measured burning time of 24 nm Al particles in water vapor [5]. To capture the size effect, a d_p^2 -law for the burning time was used [5]. The energy equation in the reaction zone was solved numerically, with the burning rate treated as the eigenvalue. Numerical integration was achieved by means of the Rosenbrock method. The Newton-Raphson iteration method was used for the root finding.

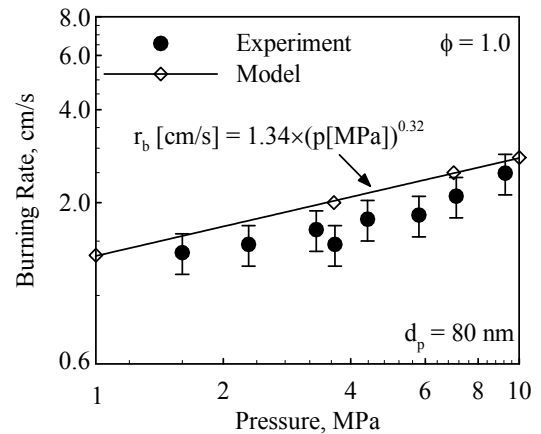


Fig. 8. Effect of pressure on burning rate of stoichiometric Al-H₂O mixtures containing 80 nm particles (reprinted from [5] with permission of Elsevier).

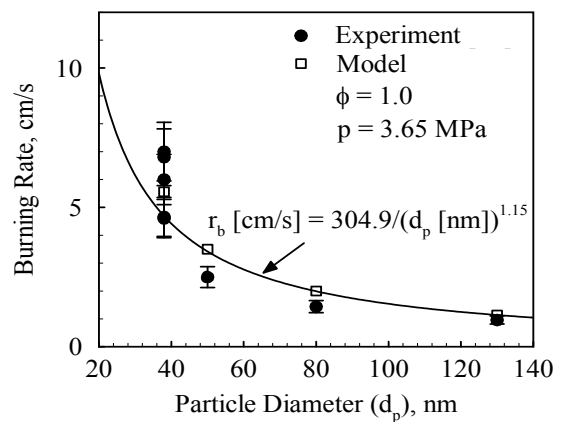


Fig. 9. Effect of particle size on burning rate of stoichiometric Al-H₂O mixture at 3.65 MPa (reprinted from [5] with permission of Elsevier).

Figures 8 and 9 show the effects of pressure and particle size on the burning rate of Al/H₂O mixtures [5]. Although the pressure and size dependencies of the burning rate were nicely captured by the model, the burning time correlation used in the analysis was not fully consistent with the experimental data. Experimental data suggest that the burning time is weakly dependent on particle size [3], contradicting the d_p^2 law used in the analysis. Note that the size effect was deduced only using three data points and there is considerable uncertainty in the size effect of the burning rate.

The previous analysis neglected many complexities such as convective motion and agglomeration of particles. It is likely that particles are entrained and transported out of the tube due to drag effects. Furthermore, particle aggregation and agglomeration is likely to occur, since temperatures as high as 2000 K were likely present. These effects were considered in the subsequent analysis [22]. The particle entrainment effect was studied by tuning the particle velocity, u_p , expressed as [22]

$$\frac{u_p}{r_b} = \left(\frac{\rho_{lw}}{\rho_{wv}} \right)^n, \tag{10}$$

where n is the entrainment index, which varies between zero (no entrainment) and unity (complete entrainment). By matching the energy fluxes in the preheat and reaction zones at $x = 0$, the following expression for the burning rate was obtained [22]

$$r_b = \sqrt{\frac{\lambda}{\rho_m C_p} \frac{2C_p(T_f - T_{ign})}{2C_p(T_{ign} - T_u) + h_{fg}} \frac{1}{\tau_b} \left(\frac{\rho_{wv}}{\rho_{lw}} \right)^n}. \tag{11}$$

The expression bears close resemblance to that obtained in our previous work, except for the factor $(\rho_{wv}/\rho_{lw})^n$.

Figure 10 shows the burning-rate pressure exponent, m , for different entrainment indices, n [22]. Particle entrainment causes the pressure exponent to increase by 0.5. This is because entrainment causes the particle velocity and reaction zone thickness to increase. Increasing the reaction zone thickness decreases the temperature gradient at the ignition point and heat flux to the preheat zone, thereby diminishing the burning rate. As the fluid velocity is pressure dependent (due to mass conservation), entrainment brings in an additional pressure dependence of the burning rate. Note that the entrainment index is expected to be dependent on mixture consistency, which can be altered by changing the particle size [7] or pH of water [16]. This is because loosely packed (or dispersed) particles are more easily entrained by the gas flow. It is thus not surprising that the mixture consistency affects the pressure exponent, as the experimental data suggest [7, 16].

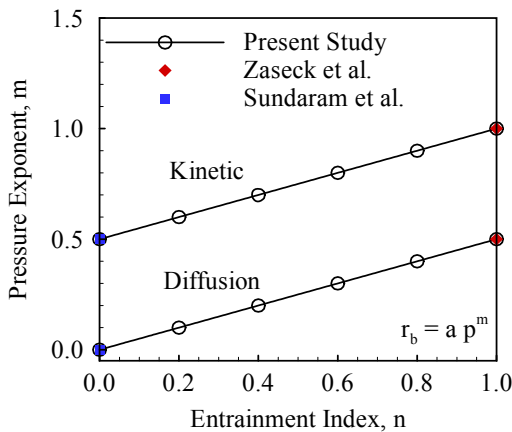


Fig. 10. Pressure exponent as a function of entrainment index for diffusion and kinetic controlled combustion mechanisms (reprinted from [22] with permission of Elsevier).

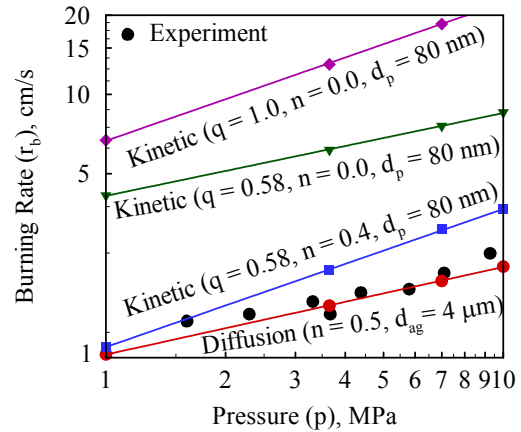


Fig. 11. Effect of pressure on the burning rate of stoichiometric aluminum-water mixture containing 80 nm particles (reprinted from [22] with permission of Elsevier).

The high temperatures and attractive forces can cause nanoparticles to aggregate, especially at high particle loading densities. Figure 11 shows the effect of pressure on the burning rate of stoichiometric aluminum-water mixture containing 80 nm particles [22]. Both diffusion and kinetically controlled conditions were considered. For the kinetics model, better agreement with experimental data was obtained, when entrainment was considered. The diffusion model offered predictions that are in reasonably good agreement with experimental data when both entrainment and agglomeration of particles were considered. It was speculated that the inverse dependence of the burning rate on particle size is caused by the combustion of particle agglomerates as opposed to original particles under diffusion-controlled conditions.

5. Conclusions

The metal-water system is attractive for propulsion and energy-conversion applications. Of all metals, aluminum has received the most attention due to its high energy density, relative safety, and low cost. Experimental studies offered new insights on the burning behaviors. Some peculiar trends were observed. The burning rate was a strong function of both pressure and particle size. The pressure exponent varied between 0 and 1, depending on the particle size, pressure, pH, and equivalence ratio. Based on the limited set of experimental data, an inverse dependence of the burning rate on particle size was proposed, although the validity of the trend is unclear. Incomplete combustion seems to be a major problem, more so for stoichiometric and

fuel-rich mixtures. Incomplete combustion also resulted in low specific impulses, thereby rendering Al/H₂O mixtures unsuitable for practical applications. Efforts to improve the performance of Al/H₂O mixtures have met with moderate success. This includes freezing the water in the mixture, using micron-sized particles, and substituting water for hydrogen peroxide.

Theoretical studies have attempted to explore the underlying physics and mechanisms.

Energy balance analysis was performed and burning rates and temperature distributions were predicted by numerical analysis. Closed-form expressions for the burning rate were also obtained. Existing models make numerous assumptions and approximations such as one-dimensional, steady state, planar, and isobaric flame propagation. Furthermore, many complexities such as entrainment and agglomeration of particles were either ignored or treated simplistically. The model is also semi-empirical and needs input of experimental data such as burning time and ignition temperature of particles. Modeling is thus in its infancy stage and existing models act only as a useful guide and not as a predictive tool.

Future works must endeavor to conduct a more rigorous analysis of metal-water combustion. To facilitate the development of a more predictive model, empiricism should be minimized. In order to capture the essential physics of the problem, a multi-phase combustion model must be developed. The model must treat complexities such as particle motion and agglomeration, radiative heat transfer and employ a more accurate reaction rate model. It should help us properly understand the existing experimental trends, offer realistic predictions for unexplored conditions, and suggest guidelines and solutions in order to realize the full potential of metal-water mixtures.

Acknowledgements

This review work was financially supported by Indian Institute of Technology Gandhinagar. The author acknowledges the financial support of U.S. Air Force Office of Scientific Research (Contract Nos. FA9550-13-1-0004 and FA9550-11-1-0002) and NASA, which enabled the author and his colleagues to conduct some of the studies discussed in this review paper during his doctoral and post-doctoral period at Georgia Institute of Technology. The author is indebted to his Ph.D. advisor, Prof. Vigor Yang, for his guidance, support, and en-

couragement. The author also wishes to thank his collaborators, Prof. Richard Yetter and Prof. Grant Risha, for their support and many intellectual discussions.

References

- [1]. D. Sundaram, V. Yang, R.A. Yetter, *Prog. Energy Combust. Sci.* 61 (2017) 293–365. DOI: 10.1016/j.pecs.2017.02.002
- [2]. D.S. Sundaram, V. Yang, V.E. Zarko, *Combust. Explos. Shock Waves* 51 (2) (2015) 173–196. DOI: 10.1134/S0010508215020045
- [3]. Y. Huang, G.A. Risha, V. Yang, R.A. Yetter, *Combust. Flame* 156 (1) (2009) 5–13. DOI: 10.1016/j.combustflame.2008.07.018
- [4]. R.A. Yetter, G.A. Risha, S.F. Son, *Proc. Combust. Inst.* 32 (2009) 1819–1838. DOI: 10.1016/j.proci.2008.08.013
- [5]. D.S. Sundaram, V. Yang, Y. Huang, G.A. Risha, R.A. Yetter, *Combust. Flame*, 160, (2013) 2251–2259. DOI: 10.1016/j.combustflame.2013.04.025
- [6]. E.W. Price and R.K. Sigman, “Combustion of aluminized solid propellants,” in Solid propellant chemistry, combustion, and motor interior ballistics, American Institute of Aeronautics and Astronautics, 2000, pp. 663–687.
- [7]. G.A. Risha, S.F. Son, R.A. Yetter, V. Yang, B.C. Tappan, *Proc. Combust. Inst.* 31 (2007) 2029–2036. DOI: 10.1016/j.proci.2006.08.056
- [8]. E. Shafirovich, V. Diakov, A. Varma, *Combust. Flame* 144 (2006) 415–418, 2006. DOI: 10.1016/j.combustflame.2005.07.018
- [9]. J. Foote, J. Lineberry, B. Thompson, B. Winkelman, “Investigation of aluminum particle combustion for underwater propulsion applications,” in 32 Joint Propulsion Conference and Exhibit, American Institute of Aeronautics and Astronautics, 1996. DOI: 10.2514/6.1996-3086
- [10]. B.J. McBride and S. Gordon. Computer Program for Calculation of Complex Chemical Equilibrium Compositions and Applications. II. User’s Manual and Program Description, Reference Publication, 1996 (Washington, DC: NASA).
- [11]. G.P. Sutton and O. Biblarz, Rocket propulsion elements. John Wiley and Sons, 2010.
- [12]. V.G. Ivanov, S.N. Leonov, G.L. Savinov, O.V. Gavrilyuk, O.V. Glazkov, *Combust. Explos. Shock Waves* 30 (1994) 569–570. DOI: 10.1007/BF00790170
- [13]. V.G. Ivanov, O.V. Gavrilyuk, O.V. Glazkov, M.N. Safronov, *Combust. Explos. Shock Waves* 36 (2000) 213–219. DOI: 10.1007/BF02699363
- [14]. G.A. Risha, T.L. Connell, R.A. Yetter, D.S. Sundaram, V. Yang, *J. Propuls. Power* 30 (2013) 133–142. DOI: 10.2514/1.B34783

- [15]. G.A. Risha, J.L. Sabourin, V. Yang, R.A. Yetter, S.F. Son, B.C. Tappan, *Combust. Sci. Technol.* 180 (2008) 2127–2142. DOI: 10.1080/00102200802414873
- [16]. D.E. Kittell, L.J. Groven, T.R. Sippel, T.L. Pourpoint, S.F. Son, *Combust. Sci. Technol.* 185 (2013) 817–834. DOI: 10.1080/00102202.2012.759948
- [17]. T.R. Sippel, T.L. Pourpoint, S.F. Son, *Propellants, Explos. Pyrotech.* 38 (2013) 56–66. DOI: 10.1002/prop.201200143
- [18]. T.L. Connell, G.A. Risha, R.A. Yetter, G. Young, D.S. Sundaram, V. Yang, *Proc. Combust. Inst.* 33 (2011) 1957–1965. DOI: 10.1016/j.proci.2010.07.088
- [19]. D.S. Sundaram, V. Yang, T.L. Connell, G.A. Risha, R.A. Yetter, *Proc. Combust. Inst.* 34 (2013) 2221–2228. DOI: 10.1016/j.proci.2012.06.129
- [20]. J.L. Sabourin, G.A. Risha, R.A. Yetter, S.F. Son, B.C. Tappan, *Combust. Flame* 154 (2008) 587–600. DOI: 10.1016/j.combustflame.2008.05.015
- [21]. D.S. Sundaram and V. Yang, *Combust. Flame* 161 (2014) 2469–2478. DOI: 10.1016/j.combustflame.2014.03.002
- [22]. D.S. Sundaram and V. Yang, *Combust. Flame* 161 (2014) 2215–2217. DOI: 10.1016/j.combustflame.2014.01.017